35th AIAA Plasmadynamics and Lasers Conference, AIAA-2004-2724
28 June 2004 – 1 July 2004, Portland, Oregon

# Numerical Simulation of Supersonic Boundary Layer Stability with Applied Electromagnetic Field in a Weakly Ionized Flow

Varun Singh* and Xiaolin Zhong†
*University of California, Los Angeles, CA, 90095*
and
Sivaram Gogineni‡
*Innovative Scientific Solutions, Inc., Dayton, Ohio*

## 1 Abstract

This paper investigates, by direct numerical simulation, the effect of an imposed electromagnetic field on a weakly ionized supersonic boundary layer in the range of 2.7 to 3.0 in a supersonic plasma wind tunnel, located at the non-equilibrium thermodynamics laboratory, under J. W. Rich and I. Adamovich, at the Ohio State University [1]. The main emphasis of the study is on MHD effects on the supersonic boundary layer. The imposed magnetic field is generated by a magnet flush-mounted in the tunnel side wall and the electric field is generated in this supersonic flow, pre-ionized by the RF discharge, by applying a DC field using electrodes flush-mounted in the top and bottom walls, perpendicular both to the flow velocity and the magnetic field. The electrical conductivity of the flow varies between 0.1 and 0.5 mho/m. The magnetic Reynolds number of the flow is small so that the induced magnetic field is neglected. The governing equations of the MHD flow, which are the Navier-Stokes equations with the applied electromagnetic force terms, are computed by a third-order upwinded numerical scheme. A series of cases with different imposed magnetic fields, electric fields and electrical conductivity, for two different stagnation pressures at the nozzle entrance, have been investigated for the mean flow. Calculations on the second mode instability are planned. It is found that in the presence of electric fields and the absence of magnetic fields, i.e. joule heating, the flow at the centerline heats up strongly leading to retardation in the flow velocity. The boundary layer thickness also increases and the mean Mach number is brought down. In the presence of magnetic field only, it is observed that the boundary layer profile changes depending on the direction of the field and, also the effect on the boundary layer is less in magnitude compared to the effect of joule heating on the same. The magnetic field is limited in its ability to mitigate the effects of an imposed electric field on the flow field. Unsteady calculations are currently underway and comprehensive conclusions on effects of external electromagnetic fields are expected in future. We have also undertaken three dimensional calculations to understand the effects of the sidewall on the flow profile.

### Nomenclature

| | | |
|---|---|---|
| **B** | = | magnetic field vector |
| $B_x, B_y, B_z$ | = | Cartesian magnetic field components |
| $c$ | = | local speed of sound |
| $C_v$ | = | constant volume specific heat |
| e | = | total energy of fluid |
| **E** | = | electric field vector |
| $J$ | = | Jacobian of grid transformation |
| **J** | = | conduction current density |

* Graduate Student, Mechanical and Aerospace Engineering Department, Student Member, AIAA. varun@ucla.edu.
† Professor, Mechanical and Aerospace Engineering Department, Associate Fellow, AIAA
‡ Senior Engineer, Innovative Scientific Solutions Inc., Associate Fellow, AIAA

| | | |
|---|---|---|
| $k$ | = | thermal conductivity |
| $\mathbf{K}$ | = | surface electric current density |
| $M$ | = | Mach number |
| $p$ | = | pressure |
| $\mathrm{P}r$ | = | Prandtl number |
| $\mathbf{q}$ | = | heat flux vector |
| $t$ | = | time |
| $T$ | = | temperature |
| $T_r$ | = | reference temperature |
| $u,v,w$ | = | Cartesian velocity components |
| $x,y,z$ | = | Cartesian coordinates |
| $\varepsilon_e$ | = | dielectric constant in free space |
| $\gamma$ | = | ratio of specific heats |
| $\mu$ | = | dynamic viscosity |
| $\mu_e$ | = | magnetic permeability in free space |
| $\rho$ | = | density of fluid |
| $\rho_e$ | = | local electric charge density |
| $\sigma$ | = | electrical conductivity of fluid |
| $\bar{\bar{\tau}}$ | = | viscous stress tensor |

## 2 Introduction

Sustained high speed flights offer potentially revolutionary improvements in space access. Factors limiting the performance of a supersonic vehicle include aerodynamic drag and heating rates exerted on the vehicles by surrounding flow fields. Recent research has indicated that supersonic flow fields may be modified significantly by magnetic Lorentz forces through the creation and manipulation of plasma near vehicles [2]. Such concepts can be used to control supersonic flows by suppressing or enhancing supersonic boundary-layer instability and transition. The suppression of the onset of supersonic boundary layer transition can lead to a significant drag and heating reductions. MHD control of supersonic boundary layer transition presents a challenge which requires both an understanding of complex supersonic MHD flow physics involving the stability and transition of boundary layer. Currently, there have not been many studies on MHD effects on supersonic boundary layer stability and transition in a supersonic tunnel with imposed magnetic and electric fields. Such MHD effects cannot be analyzed by the popular linear stability analysis (LST) for supersonic boundary layers because the MHD effects can alter the mean flow profiles substantially invalidating the parallel flow assumption used for LST.

### 2.1 MHD effects on Weakly Ionized Supersonic Flows

In supersonic flows, the gas becomes weakly ionized either by viscous heating or by artificially generating plasma in the flow. If there is an imposed electromagnetic field in the flow, the flow properties can be changed substantially by the interaction of the electrically conducting gas and the electromagnetic field. Such interaction forms the basic idea of electromagnetic flow of supersonic flow. Many researchers have shown that supersonic flow can be altered significantly by Lorentz force [3-9]. It was found that MHD effects weaken the bow shock structure and significantly reduce the shock standoff distance for supersonic flow over a blunt body with the presence of an imposed magnetic field.

Rossow [10] first studied the incompressible boundary layer flow over a flat plate in the presence of a uniform magnetic field applied normal to the plate. The electrical conductivity was assumed to be constant. The MHD boundary-layer equations were solved by numerical integration. He found that the skin friction and heat-transfer rates were reduced when the transverse magnetic field was fixed to the plate, but increased when the magnetic field was fixed to the moving fluid. In both cases, the total drag was found to be increased. Bleviss [11] investigated MHD effects on hypersonic Couette flow in which a uniform magnetic field normal to the wall was externally imposed. Assuming variations of electrical conductivity, viscosity, and Prandtl number with temperature, the flow was solved exactly with minimum assumptions about the gas. The results for the case of thermally insulated wall showed a tremendous decrease in skin friction and significant increase in total drag with reasonable magnetic field strength. It was also found that the temperature increased across the flow field and heat transfer increased at the moving wall.

For the heat transfer case, a significant increase in total drag was accompanied by a moderate increase in the heat transfer. Palm et al. [1] experimentally studied MHD effect on a supersonic weakly ionized flow. The results showed a reproducible effect of the $j \times \mathbf{B}$ force on the pressure fluctuation spectra in the test section of a supersonic tunnel. The pressure fluctuation intensity decreased for the retarding Lorentz force.

Effects of MHD on boundary-layer stability were investigated by Rossow [12] using a linear stability analysis. The effectiveness of a magnetic field in stabilizing the laminar flow on an incompressible, electrically conducting fluid was studied. Rossow found that flow over a flat plate was stabilized by either a coplanar or transverse magnetic field fixed relative to the fluid. He attributed the destabilizing effect to the inherently unstable velocity profile induced by the magnetic field. Cheng et al. [13] numerically investigated the effect of an applied magnetic field on the instability of Mach 4.5 boundary layer over a flat plate. Assuming a constant electrical conductivity of 100 mho/m and absence of joule heating, the imposed magnetic fields significantly decelerated the boundary layer. An adverse pressure gradient was created in some regions strong enough to cause flow separation. The unsteady calculations showed MHD effects substantially stabilized the second mode instability where the mean flow boundary was modified, despite adverse pressure gradient and local flow separation.

### 2.2 Supersonic Boundary Layer Instability

The transition process in boundary layers is the result of the nonlinear response of the laminar boundary layers to forcing disturbances [14]. In an environment with small initial disturbances corresponding to those encountered in hypersonic flights, the paths to transition consist of three stages: 1) receptivity, 2) linear eigenmode growth or transient growth, and 3) non-linear breakdown to turbulence. The process of instability and transition is much more complex and much less understood for hypersonic boundary layers than for low-speed incompressible boundary layers. Most of our knowledge on the stability properties of hypersonic boundary layers is obtained by the analyses of local parallel linear stability theory (LST) [15, 16]. Lees and Lin [17] showed that the existence of a generalized inflection point is a necessary condition for inviscid instability of a compressible boundary layer. Mack [15] found that there are higher acoustic instability modes in addition to the first-mode instability waves in supersonic and hypersonic boundary layers. The dominance of the second mode have been validated by experimental stability studies [18] Currently, it is not known how an imposed electromagnetic field will affect a supersonic boundary layer in an experimental set up and the stability characteristics of the second mode.

### 2.3 DNS of Supersonic Boundary Layer Instability

Due to the difficulty in conducting ground-based supersonic experiments and the complexity of supersonic flows, the approach of direct numerical simulation (DNS) without empirical turbulence models is a potentially powerful tool in studying and understanding supersonic and hypersonic flow physics for the development of future hypersonic space vehicles. In DNS studies, the full unsteady Navier-Stokes equations are numerically simulated without using any empirical turbulence models. The development of instability waves and nonlinear breakdown are numerically captured by the simulation. Though such a simulation is computationally intensive, it has the ability to simulate many of the effects that are neglected by parallel linear stability theory (LST) and parabolic stability equations (PSE) [19].

Erlebacher et al. [20, 21] studied the secondary instability mechanism of compressible boundary layers over a flat plate by temporal and spatial direct numerical simulation. Thumm et al. [22], Fasel et al. [23], and Eibler et al. [24, 25] performed spatial DNS of the oblique breakdown of transition in a supersonic boundary layer over a flat plate based on compressible 3-D Navier-Stokes equations. Adams and Kleiser [26, 27] studied the subharmonic transition process of a flat-plate at a freestream Mach number of 4.5 by temporal direct numerical simulation. Pruett et al. [28-30] performed spatial simulations for supersonic boundary layers over flat plates and sharp cones. The results are compared with parabolic stability equations (PSE). Cheng et al. [13] performed a DNS study of the effect of applied magnetic field on the instability of Mach 4.5 boundary layer over a flat plate. All these DNS studies on compressible boundary layers show that the DNS of high-speed boundary layer transition is feasible on existing computers using efficient and accurate numerical methods. They can provide detailed information which can not be obtained by other means for the study of transition of hypersonic boundary layers.

In the past several years, Zhong and his colleagues at UCLA have been developing new fifth and higher order numerical simulation methods and computer codes for the simulation studies of supersonic and hypersonic boundary layer stability and transition in non-trivial geometries with bow shock effects [31]. We have also conducted numerical studies of the receptivity and stability of a number of 2-D and 3-D hypersonic flows over blunt bodies [32].

The numerical simulations as well as other supporting theoretical approaches are used to gain a fundamental understanding of the physical mechanism of laminar-turbulent transition of hypersonic boundary layers over complex 3-D maneuvering vehicles affected by shock waves and real-gas effects. The numerical tools developed in these studies are extended to the current study of MHD effects of the second mode instability.

### 2.4 Scope of Current Study

The study by Rossow was done before the discovery of the second instability mode in a supersonic boundary layer by Mack [15]. It has been generally recognized that the second mode is the most dangerous mode in high Mach number boundary layers. Cheng at al. [13] studied the effects of an applied magnetic field on a Mach 4.5 boundary layer over a flat plate. However, the combined effects of an electromagnetic field on a supersonic boundary layer in an actual experimental set up have not been studied. Therefore, the objective of this paper is to investigate electromagnetic effects on the supersonic boundary layer in a plasma wind tunnel, mirroring the flow conditions of the experiments, which are being conducted at the non-equilibrium thermodynamics laboratory, by J. W. Rich and I. Adamovich at the Ohio State University [1].

DNS approach is chosen because LST may not apply on the highly nonparallel mean flow distorted by the applied magnetic and electric fields. In this paper, a supersonic flow in a three-dimensional expanding test section, with slightly divergent sidewalls, is studied, using numerical simulation, under an externally imposed electromagnetic field. We propose to simulate an array of scenarios with a variation in the magnetic field strength, electric field strength and electrical conductivity for two different plenum pressures of one atmosphere and one-third atmosphere. The imposed magnetic field is produced by a permanent magnet, 5 cm in length and as wide as the side wall, starting 10 cm downstream from the entrance of the tunnel flush mounted in the nozzle side wall. The transverse DC electrical current is spatially superimposed on the magnetic field using two copper electrodes flush mounted in the top and bottom nozzle walls, perpendicular to the magnetic field and the flow direction. The governing equations for the MHD flow are formulated from the Navier-Stokes and the Maxwell equations, and are spatially discretized by our third-order numerical scheme. In an attempt to solve the coupled MHD equations, difficulties were encountered due to the constraint of the size of time step posed by the magnetic diffusivity of the magnetic induction equation. To resolve the “stiffness" problem, we solve the approximate MHD equations without the induction equation by neglecting the induced magnetic field and assuming that the imposed magnetic field is constant. This is actually a fair assumption considering that the magnetic Reynolds number is in the order of $10^{-3}$.

## 3 Governing Equations

The governing equations of MHD of compressible flow are the Maxwell equations coupled with the Navier-Stokes equations through the momentum and energy equations. The current density **J** in MHD is given by the generalized Ohm's law as follows,

$$\mathbf{J} = \sigma(\mathbf{E} + \mathbf{u} \times \mathbf{B}) \tag{1}$$

where **E** is the electric field vector and σ is the electrical conductivity. This equation relates the current density with the electric field and the induced electric field generated by crossing the magnetic field lines with the velocity vector. This form of the electric current equation neglects the Hall current for simplicity. In this paper, in order to solve the MHD equations more efficiently, we only consider the cases where the small magnetic Reynolds number assumption applies. The magnetic Reynolds number defined as $UL\sigma\mu_e$ is in the order of $10^{-3}$ for all cases presented in this paper, where σ is the electrical conductivity of fluid and $\mu_e$ is the magnetic permeability in free space. Since it is much less than unity, we assume that the induced magnetic field is negligible and the imposed magnetic field is constant through all the computations.

The set of MHD equations with the assumption of negligible induced magnetic field are written as follows:

$$\frac{\partial \rho}{\partial t} + \nabla.(\rho \mathbf{u}) = 0 \tag{2}$$

$$\rho\left(\frac{\partial \mathbf{u}}{\partial t}+\mathbf{u}\cdot\nabla\mathbf{u}\right)=-\nabla p+\nabla\cdot\overline{\overline{\tau}}+\sigma(\mathbf{E}\times\mathbf{B})+\sigma(\mathbf{u}\times\mathbf{B})\times\mathbf{B} \tag{3}$$

$$\frac{\partial e}{\partial t}+\nabla\cdot(e\mathbf{u})=-\nabla\cdot(p\mathbf{u})+\nabla\cdot(\mathbf{u}\cdot\overline{\overline{\tau}})-\nabla\cdot\mathbf{q}+\mathbf{E}\cdot\mathbf{J} \tag{4}$$

where $e=\frac{p}{(\gamma-1)}+\frac{1}{2}\rho U^2$ , is the internal energy plus the kinetic energy of the fluid. The viscous stress and the heat flux are given by the usual constitutive equations in Newtonian fluid as follows

$$\tau_{ij}=\mu\left(\frac{\partial u_i}{\partial x_j}+\frac{\partial u_j}{\partial x_i}\right)-\frac{2}{3}\mu\frac{\partial u_k}{\partial x_k}\delta_{ij} \tag{5}$$

$$q_i=-k\frac{\partial T}{\partial x_i} \tag{6}$$

Where μ is the viscosity coefficient determined by the Sutherland law,

$$\mu=\mu_r\left(\frac{T}{T_r}\right)^{\frac{3}{2}}\frac{T_r+T_s}{T+T_s} \tag{7}$$

Where $T_r$ = 288K, $T_s$ = 110K, and $\mu_r$ = 0.17894 × $10^{-4}$ kg/m/s for air. The thermal conductivity k is computed from the Prandtl number, which is assumed constant and it takes the value of 0.72 in this paper.

The imposed magnetic field is taken as spatially and temporally uniform in a direction perpendicular to the flow vector in the span wise direction for simplicity. The electric field is spatially and temporally uniform in a plane perpendicular to the flow vector and the magnetic field vector for simplicity.

## 4 Numerical Method

There have been several recent works on developing upwind schemes for MHD equations with shock capturing capability [33, 34]. Most of these methods are second order accurate TVD schemes, which may not be accurate enough for the numerical simulation of instability waves in supersonic boundary layer. Such simulation requires high-order numerical accuracy in order to capture a wide range of time and length scales in the wave fields. Since our goal is to analyze the stability of supersonic boundary layer with MHD effects, it is necessary to use a high-order and robust numerical scheme for the numerical simulation. Therefore, we use a third-order finite difference scheme that we have developed and validated for solving the full Navier-Stokes equation for spatial discretization of the MHD equations [31]. The numerical method used in this study is briefly summarized in this section. More details on the method and its validations can be found in [31].

In numerical simulation, the MHD equations (2) to (4) are written in the following conservative form,

$$\frac{\partial U}{\partial t}+\frac{\partial E}{\partial x}+\frac{\partial F}{\partial y}+\frac{\partial G}{\partial z}+\frac{\partial E_v}{\partial x}+\frac{\partial F_v}{\partial y}+\frac{\partial G_v}{\partial z}=M \tag{8}$$

Where U is the solution vector given by

$$U=\{\rho,\rho u,\rho v,\rho w,e\} \tag{9}$$

*E, F, G* are the inviscid flux terms, and $E_v$, $F_v$, $G_v$ are the viscous terms, and *M* is the MHD source term. They are written as follows

$$E = \begin{Bmatrix} \rho u \\ \rho u^2 + p \\ \rho uv \\ \rho uw \\ (e+p)u \end{Bmatrix} \tag{10}$$

$$F = \begin{Bmatrix} \rho v \\ \rho vu \\ \rho v^2 + p \\ \rho vw \\ (e+p)v \end{Bmatrix} \tag{11}$$

$$G = \begin{Bmatrix} \rho w \\ \rho wu \\ \rho wv \\ \rho w^2 + p \\ (e+p)w \end{Bmatrix} \tag{12}$$

$$E_v = \begin{Bmatrix} 0 \\ \tau_{xx} \\ \tau_{yx} \\ \tau_{zx} \\ u\tau_{xx} + v\tau_{yx} + w\tau_{zx} - q_x \end{Bmatrix} \tag{13}$$

$$F_v = \begin{Bmatrix} 0 \\ \tau_{xy} \\ \tau_{yy} \\ \tau_{zy} \\ u\tau_{xy} + v\tau_{yy} + w\tau_{zy} - q_y \end{Bmatrix} \tag{14}$$

$$G_v = \begin{Bmatrix} 0 \\ \tau_{xz} \\ \tau_{yz} \\ \tau_{zz} \\ u\tau_{xz} + v\tau_{yz} + w\tau_{zz} - q_z \end{Bmatrix} \tag{15}$$

$$M = \sigma \begin{Bmatrix} 0 \\ -u\left(B_y{}^2 + B_z{}^2\right) + v\left(B_x B_y\right) + w\left(B_x B_z\right) + E_y B_z - E_z B_y \\ u\left(B_x B_y\right) - v\left(B_x{}^2 + B_z{}^2\right) + w\left(B_y B_z\right) + E_z B_x - E_x B_z \\ u\left(B_x B_z\right) + v\left(B_y B_z\right) - w\left(B_x{}^2 + B_y{}^2\right) + E_x B_y - E_y B_x \\ E_x{}^2 + E_y{}^2 + E_z{}^2 + v\left(E_x B_z - E_z B_x\right) + w\left(E_y B_x - E_x B_y\right) + u\left(E_z B_y - E_y B_z\right) \end{Bmatrix} \tag{16}$$

In the conservative equation (8), the inviscid fluxes and the viscous fluxes have the same forms as those of the Navier-Stokes equations. The new term, M, represents the contribution of the Lorentz force.

Before discretizing the governing equations by a finite difference method, equation (8) in the physical domain is transformed to the body-fitted computational domain by the following transformation relations,

$$\begin{cases} \xi = \xi(x, y, z) \\ \eta = \eta(x, y, z) \\ \varsigma = \varsigma(x, y, z) \\ \tau = t \end{cases} \Leftrightarrow \begin{cases} x = x(\xi, \eta, \varsigma, \tau) \\ y = y(\xi, \eta, \varsigma, \tau) \\ z = z(\xi, \eta, \varsigma, \tau) \\ t = \tau \end{cases} \tag{17}$$

And the transformed governing equation in the computational domain is expressed as follows

$$\frac{1}{J}\frac{\partial U}{\partial \tau} + \frac{\partial E'}{\partial \xi} + \frac{\partial F'}{\partial \eta} + \frac{\partial G'}{\partial \varsigma} + \frac{\partial E'_v}{\partial \xi} + \frac{\partial F'_v}{\partial \eta} + \frac{\partial G'_v}{\partial \varsigma} + U\frac{\partial\left(\frac{1}{J}\right)}{\partial \tau} = M \tag{18}$$

A third-order explicit finite difference scheme is used for spatial discretization of the governing equation (18), the inviscid flux terms are discretized by the upwind scheme, and the viscous flux terms are dicretized by the central scheme. For the inviscid flux vectors, the flux Jacobians contain both positive and negative eigenvalues, a simple local Lax-Friedrichs scheme is used to split vectors into negative and positive wave fields. For example, the flux term F′ in Eq (18) can be split into two terms of pure positive and negative eigenvalues as follows

$$F' = F'_+ + F'_- \tag{19}$$

Where $F'_+ = \frac{1}{2}\left(F' + \lambda U\right)$and $F'_+ = \frac{1}{2}\left(F' - \lambda U\right)$ and λ is chosen to be larger than the local maximum eigenvalue of F′.

$$\lambda = \frac{|\nabla \eta|}{J}\left(\sqrt{(\varepsilon c)^2 + u'^2} + c\right) \tag{20}$$

where

$$u' = \frac{\eta_x u + \eta_y v + \eta_z w + \eta_t}{|\nabla \eta|} \tag{21}$$

The parameter ε is a small positive constant added to adjust the smoothness of the splitting. The fluxes $F'_+$ and $F'_-$ contain only positive and negative eigenvalues respectively. Therefore, in the spatial discretization of equation (18 ), the derivative of the flux F is split into two terms

$$\frac{\partial F'}{\partial \eta} = \frac{\partial F'_+}{\partial \eta} + \frac{\partial F'_-}{\partial \eta} \tag{22}$$

Where the first term on the right hand side is the discretized by the upwind scheme and the second term by the downwind scheme.

## 5 Boundary Conditions

The computational domain is weakly ionized supersonic flow over a flat plate with an imposed electromagnetic field. The upper boundary of the domain is the half-line of the supersonic tunnel which is a plane of symmetry. The boundary conditions are described below.

### 5.1 Upper Boundary

Exploiting the symmetry of the supersonic tunnel, only the lower half of the physical domain is computed. The upper boundary serves as a horizontal plane of symmetry for all flow variables. The imposed electromagnetic field has no effect at the plane of symmetry.

### 5.2 Lower Boundary

The wall of the tunnel itself is the lower computational boundary, it is assumed to be adiabatic so that $\frac{\partial T}{\partial y} = 0$ is enforced at the boundary. The velocity components *u* and *w* are zero following the non-slip wall condition and *v* is zero according to the solid-wall condition. For the magnetic field lines across the lower boundary, the normal component of the magnetic field across the wall is continuous. The tunnel wall is assumed non-magnetic such that the tangential component across the boundary is given by

$$\hat{\mathbf{n}} \times (\mathbf{B_2} - \mathbf{B_1}) = \mu_e \mathbf{K} \tag{23}$$

Where $\hat{\mathbf{n}}$ is the surface normal vector and **K** is the surface current density. We assume that the wall is electrically insulated, therefore the surface current density is zero and the tangential component of the magnetic field is continuous across the wall.

### 5.3 Left Boundary

The far side boundary serves as a vertical plane of symmetry for all flow variables in the span wise direction. Only one half of the physical domain in the span wise direction is computed. The electromagnetic field has no effect at the plane of symmetry.

5.4 Right Boundary

The near side boundary of the computational domain is the wall of the tunnel. It is assumed to be adiabatic, i.e. $\frac{\partial T}{\partial z} = 0$ is enforced at the boundary. The velocity components *u* and *v* are zero following the non-slip condition and *w* is zero according to the solid-wall condition. For the magnetic field lines across the near side boundary, the normal component of the magnetic field across the wall is continuous. The tunnel wall is assumed non-magnetic such that the tangential component across the boundary is given by

$$\hat{\mathbf{n}} \times (\mathbf{B}_2 - \mathbf{B}_1) = \mu_e \mathbf{K} \tag{24}$$

where $\hat{\mathbf{n}}$ is the surface normal vector and **K** is the surface current density. We assume that the wall is electrically insulated, therefore the surface current density is zero and the tangential component of the magnetic field is continuous across the wall.

5.5 Inlet and Exit conditions

The inlet conditions are fixed and are given by the initial conditions of the flow based on a boundary layer solution. At exit, the flow variables are extrapolated from the interior points as done in [31].

## 6 Flow Conditions

In this paper, a high speed weakly ionized viscous flow in a supersonic wind tunnel in various imposed electromagnetic fields is considered. We consider two different plenum pressures, i.e. one-third atmospheric pressure and one atmospheric pressure and several cases of magnetic fields, electric fields and electrical conductivities. The flow conditions that stay uniform are $M_\infty$= 2.75, $T_\infty$=288K and $Pr$=0.72. The focus of the study is on to study the effects of varying MHD forces on the supersonic boundary layer. To verify the grid independence of the results, we ran the base steady case for two different grid sizes, i.e. 121 by 120 and 121 by 60. Figure 1 shows the results from these calculations. Figure 1(a) shows a comparison of the Mach number distribution along the centerline for the two grids and figure 1(b) shows the comparison of temperature at the tunnel centerline. Clearly, the results are independent of the grid sizes within an admissible limit. To evaluate the effects of MHD and joule heating on the flow characteristics, we have established steady flow solutions. Figure 2 shows the schematic of velocity vectors through the MHD tunnel, in the absence of any externally imposed electric or magnetic fields. The isocontours of Mach number, pressure and temperature are shown in Figures 3(a) through 3(c). Our initial calculations were for a plenum pressure of one atmospheric pressure. However, the set of results presented here is for a plenum pressure of one-third atmospheric pressure. At a lower plenum pressure of one-third atmospheric pressure, the boundary layer thickness becomes nearly twice that at one atmospheric pressure making it more sensitive to the external fields and this enhances our understanding of the effects of those external fields. Figure 4(a) shows the comparison of the boundary layer thicknesses at two different plenum pressures and it supports our conclusion. In figure 4(b), it is clear that the Mach number profile at the centerline is not significantly affected. Figures 5(a) and (b) show a comparison of pressure at the centerline. Figure 5(b) is a zoomed in view of 5(a) which increases our visualization of the pressure distribution at the centerline. All pressure data now presented will be a similar view for enhanced visualization.

In the current simulation, the tunnel is a little less than 0.21m in length. The vertical width of the tunnel at its entrance is a little less than 5mm. The external fields are imposed between 0.104m and 0.156m downstream of the tunnel entrance. The spatially uniform electric field, which always points in the positive vertical direction, exists between those two points in our tunnel. The magnetic field acts in the span wise direction between those two locations in our tunnel. In our calculations, to study the effects of magnetic field directions, we reverse the directions of this magnetic field. Figure 6(a) shows the schematic of the fields imposed.

To increase the efficiency of our calculations, we utilized the inherent symmetry of the tunnel about a horizontal plane. Therefore, our two-dimensional computational domain constitutes of the lower half of the actual tunnel which is divided by a horizontal plane at the centerline. Similarly, for our three-dimensional calculations, we divided the tunnel using two planes of symmetry along a symmetric vertical and a horizontal plane. This helps us greatly reduce the computational expense of our calculations. For the two-dimensional case, the computational

domain in our calculations is resolved by 121 uniform grids in the horizontal direction and 120 stretched grids in the vertical direction. Figure 6(b) shows the grid used for calculating the two-dimensional flow field.

In our simulations, we consider several combinations of electric and magnetic fields to understand the effects of these external fields on the boundary layer. First we look at the effects of increasing electric fields on the flow parameters in the tunnel test section at a constant electric conductivity of 0.5mho/m. Following this, we look at the mitigating effects of the magnetic field on joule heating. Finally, we look at the effects of reversing the magnetic field direction on the boundary layer thickness, Mach number, temperature and pressure at the centerline for various cases. For the unsteady cases, we have imposed a blowing and suction disturbance on the wall, 0.11m downstream of the tunnel entrance. The disturbance frequency is 20kHz.

The effects of imposed electromagnetic fields on steady and unsteady flow are investigated numerically and presented in the following sections.

## 7 MHD Effects on Steady Flow Solutions

The effects of an imposed electric and magnetic field on steady supersonic boundary-layer flow over a flat plate are first studied. In the experimental facility, the magnetic field is generated using a magnet flush mounted in the side wall of the tunnel. The transverse electric field in the supersonic flow pre-ionized by the RF discharge is sustained by applying a DC field by two electrodes flush mounted in the top and the bottom nozzle walls.

The results for the steady flow cases are divided into three different sets of cases in an attempt to study the effects of the imposed fields in isolation. This gives us a better understanding of the individual effects of the magnetic and electric fields on the flow fields.

### *7.1 Case I. Effects of varying electric fields in absence of magnetic fields at constant electrical conductivity*

We first consider the case of Mach 2.7 to 3.0 flows in the test section of the tunnel in the absence of magnetic fields. The electrical conductivity of the weakly ionized flow is maintained constant at 0.5mho/m. The electric field points vertically upwards, i.e. positive y-direction, at all times and is constant, both spatially and temporally. The five values of electrical fields computed here are 1500V/m, 2000V/m, 2500V/m, 3000V/m and 3500V/m. The electrical fields are imposed on the bottom and the top walls of the test section between 0.104m and 0.156m downstream of the tunnel entrance.

Numerical results of the steady supersonic flow, in the neighborhood of Mach 3.0 at the centerline in the test section, are obtained using a third-order scheme. The results are shown in figure 7. In general, with increasing electric field, the effects of joule heating are seen to increase for constant electrical conductivity. The stronger electric fields alter the flow field more significantly than the weaker electric fields. There is significant rise of temperature, in the boundary layer, in the regions where the electric field is imposed. The pressure at the centerline is altered with increasing electric field strength.

Figure 7 compares the effects of varying electric fields in the temperature, Mach number and pressure at the centerline and the boundary layer profile at the tunnel exit, downstream of the location electric fields. The highest electric field of 3500V/m retards the flow at the centerline more strongly than the lowest electric field of 1500V/m. This effect reduces with decreasing electric fields in that range of 3500V/m and 1500V/m. The temperature at the centerline also shows the most drastic increase for 3500V/m when compared to the cold flow temperature at the centerline. The difference goes down with decreasing electric fields as is evident from the figure. The pressure behaves in a pattern identical to temperature. It goes up with increasing electric field strength as is seen in figure 7(c). Finally, comparing the boundary layer profiles at the exit of the tunnel entrance and downstream of the imposed electric fields, we notice that the electric field leads to a significant retardation in the mean flow Mach number in the nozzle test section. Another observation is the thickening of the boundary layer thickness with the imposition of an electric field. It is evident that, with an increasing electric fields, these effects increase in magnitude. With 3500V/m, the mean Mach number in the test section is the lowest, and in fact drops from 2.9 for cold flow to a little over 2.5. Similarly, the boundary layer goes through an observable increase in its thickness for the highest electric field of 3500V/m.

### *7.2 Case II. Effect of a constant electric field on a flow field with and without external magnetic field.*

In this case, we picked an electric field of 2000V/m with an electrical conductivity of 0.1mho/m through out the flow. The electrical conductivity is brought down from 0.5mho/m in the flow field, in the previous case, to 0.1mho/m to help us distinguish the mitigating effects of magnetic field on the flow already altered by the electric

field. We have imposed a magnetic field of 1.5T throughout the flow field in the span wise direction, along the positive z-direction. The results are shown in figure 6. In general, it is seen that the imposition of the magnetic field accelerates the flow that has been previously retarded by the imposition of an electric field. However, the effects of a high magnetic field of 1.5T are not enough to strongly nullify the effects of joule heating.

Figure 8(a) shows the comparison of the Mach number at the centerline of the tunnel. It clearly shows that the mitigating effect of a high magnetic field of 1.5T is relatively small. Similarly, in figure 8(b) which compares the Mach numbers at the centerline of the tunnel, a trend similar to temperature is seen. Figure 8(c) compares the pressure distribution at the centerline of the tunnel and the changes in profile due to an added magnetic field are insignificant as present magnitude of magnetic field strength. Figure 8(d) compares the Mach number profile at the exit of the tunnel for the three cases. It is evident from the figure that the magnetic field, at its current magnitude of 1.5T, is capable of overcoming the strong effects if a very high external electric field is imposed.

### *7.3 Case III. Effects of reversing the magnetic field direction on flow altered by varying electric fields.*

We next consider flow altered by the presence of two independent electric fields 2000V/m and 3000V/m in magnitude. The fields are constant and point in the positive y-direction. The electrical conductivity is 0.1mho/m for both the electric fields. We imposed a magnetic field of 1.5T, in the positive and negative z-direction for both cases of electric fields to establish the effects of reversing the magnetic field direction in conjunction with varying magnitude of electric fields. The measurements are taken at the exit of the tunnel. In general, we observe that depending on the direction of the magnetic field imposed, the flow either gets accelerated or retarded. Also, this effect is more pronounced at higher values of electric fields for the same magnitude of magnetic field.

Figures 9(a) and (b) show a comparison of temperature at the centerline of the tunnel for the two cases of electric fields, i.e. 2000V/m and 3000V/m. In figure 9(a), it is clear that the flow altered by the electric field of 2000V/m is heated by a positive magnetic field of 1.5T and cooled by a negative magnetic field of the same magnitude. Figure 9(b) shows that with the same magnitude of magnetic fields but a higher electric field of 3000V/m, the effect of temperature increase and reduction due to reversed directions of magnetic field are stronger. Figures 10(a) and (b) show a comparison of Mach number profiles at the centerline of the tunnel for the two cases of electric fields, i.e. 2000V/m and 3000V/m. At 2000V/m, the effects of retardation and acceleration of the flow at the centerline are visible but not strong enough. However, at a higher electric field of 3000V/m the same effects become more discernable. Figures 11(a) and (b) show a comparison of the Mach number profile at the exit of the tunnel. Once again, the higher electric field in combination with the same magnetic field is able to produce a significant alteration in the flow. Figures 12(a) and (b) compare the distribution of pressure at the centerline under the two different cases examined here. The pressure, again showing a behavior similar to temperature, gets mitigated by the positive magnetic field and rises under a negative magnetic field.

For all cases considered, we see that electric fields have a similar retarding effect on the supersonic flow field. It is evident that higher electric fields lead to a greater affect on the flow field. They also lead to a rise in the temperature at the centerline and thickening of the boundary layer. The magnetic field is capable of mitigating the effects of joule heating, depending on its orientation. At lower electric fields, this effect is relatively weak. A fixed magnetic field when applied in combination with high magnitude of electric field can produce significant changes in the weakly ionized supersonic flow.

## 8 MHD effects on unsteady flow cases with imposed wall disturbances

The steady flow solutions presented in the previous section show substantial alterations of the boundary layer structure and the mean flow by imposed magnetic fields. Efforts to determine the effects of the combination of electric and magnetic fields on the stability of the supersonic boundary layer are currently underway.

Figure 13 shows the isocontours of disturbances in the Mach number and pressure when a wall blowing and suction is imposed 0.11m downstream of the tunnel entrance. The frequency imposed is 20 kHz. Currently calculations are underway for higher frequencies and effects of electromagnetic fields on those disturbances.

## 9 Summary and Conclusions

Weakly ionized supersonic flow in a tunnel in presence of a number of imposed electromagnetic fields was studied by DNS. The main focus was on the joule heating and MHD effects on the steady state solutions in the test section of the high speed tunnel.

The steady flow results show that all imposed electromagnetic fields significantly alter the boundary layer profile. For high electric fields in isolation of the magnetic field, localized heating in the vicinity of the electric field is observed. Imposed electric fields can significantly alter the flow properties at the centerline of the tunnel. High electric fields can be particularly traumatic and retard the mean flow significantly.

With a constant electric field and magnetic field strength, significant alterations can be produced in the flow field by changing the electrical conductivity. Higher electrical conductivities for fixed field strengths will lead to greater changes in the flow than lower conductivities for the same fields.

For mitigating the effects of a high electric field, the magnetic field strength required is significant and it is observed that joule heating is stronger in altering the flow field when compared to the effects of magnetic field in absence of electric fields. However, at high electric fields and electrical conductivity, even a moderate magnetic field can alter the flow field significantly.

It should be pointed out that this is an initial numerical study of an experimental investigation of weakly ionized supersonic flows in a tunnel, with constant electric conductivities, electric fields and magnetic fields, and a combination of the above. Further and more extensive studies are currently underway by the authors to study the effects of electromagnetic fields on steady state and their effects on wall disturbances.

**Acknowledgements:** *This research was supported by Innovative Scientific Solutions Inc., Dayton, Ohio and the Air Vehicles Directorate of Air Force Office of Scientific Research, under an SBIR Phase II grant. The authors would like to thank Dr. J W Rich, I Adamovich of the Ohio State University and Dr. R L Kimmel of the Air Force Research Laboratory, Dayton, Ohio for their valuable suggestions during the course of this work.*

## References

[1] Palm, P., Meyer, R., Plönjes., E., Bezant, A., Adamovich, I., Rich, J. W. and Gogineni, S.,"MHD effect on a supersonic weakly ionized flow,"*AIAA-2002-2246,* 2002

[2] Shang, J.S., "An Outlook of CEM Multidisciplinary Applications," *AIAA Paper 99-0336,* 1999.

[3] Canupp, P. W., "The influence of magnetic fields for shock waves and hypersonic flows," *AIAA Paper 2000-2260,* 2000.

[4] Damevin, H., Dietiker, J., and Hoffmann, K. A.," Hypersonic flow computations with magnetic field," *AIAA Paper 2000-0451,* 2000.

[5] Agarwal, R. K., and Augustinus, J.,"Numerical simulation of compressible viscous MHD flows for reducing supersonic drag of blunt bodies," *AIAA Paper 99-0601,*1999.

[6] Hoffmann, K. A., Damevin, H., and Dietiker, J.,"Numerical simulation of hypersonic magnetohydrodynamic flows," *AIAA paper 2000-2259,* 2000.

[7] Poggie, J., and Gaitonde, D. V.,"Magnetic control of hypersonic blunt body flow," *AIAA paper 2000-0452,* 2000.

[8] Gaitonde, D. V., "Development of solver for 3-D nonideal magnetogasdynamics," *AIAA paper 99-3601,* 1999.

[9] Shang, J. S., Canupp, P. W. and Gaitonde, D. V."Computational magneto-aerodynamic hypersonics,"*AIAA paper 99-4903,* 1999.

[10] Rossow, V. J.,"On flow of electrically conducting fluids over a flat plate in the presence of a transverse magnetic field,"*NACA TN 3971,* 1957.

[11] Bleviss, Z. O.,"Magnetogasdynamics of hypersonic Couette flow,"*Journal of the Aero/Space Sciences,* Vol. 25 no 10, 1958, pp. 601-615.

[12] Rossow, V. J, "Boundary-layer stability diagrams for electrically conducting fluids in the presence of a magnetic field,"*NACA TN 4282,* 1958.

[13] Cheng, F., Zhong, X., Gogineni, S. and Kimmel, R. L., "Effect of applied magnetic field on the instability of Mach 4.5 boundary layer over a flat plate," *AIAA paper 2002-0351,* 2002

[14] Reshotko, E., "Boundary Layer Instability, Transition and Control,"*AIAA paper 94-0001*, 1996.

[15] Mack, L. M.,"Boundary Layer Linear Stability Theory,"*AGARD report, No. 709,* 1984, pp. 3-1 to 3-81.

[16] Malik, M. R.,"Prediction and Control of Transition in Hypersonic Boundary Layers" *AIAA Paper 87-1414,* 1987.

[17] Lees, L. and Lin, C. C."Investigation of the Stability of the Laminar Boundary Layer in Compressible Fluid," *NACA TN No. 1115,* 1946.

[18] Stetson, K. F. and Kimmel, R. L. "On Hypersonic Boundary Layer Stability," *AIAA paper 92-0737,* 1992.

[19] Herbert, T.,"Parabolized Stability Equations," *In Progress in Transition Modeling, AGARD-FDP-VKI Special Course,* 1993.

[20] Erlebacher, G., and Hussaini, M. Y.,"Numerical Experiments in Supersonic Boundary-Layer Stability," *Physics of Fluids:* A, Vol. 2, 1990, pp. 94-104.

[21] Ng, L. L., and Erlebacher, G.,"Secondary Instability in Compressible Boundary Layers,"*Physics of Fluids:* A, Vol. 4, 1992, pp. 710-717

[22] Thumm, A., Wolz, W. and Fasel, H.,"Numerical Simulation of Spatially Growing Three-Dimensional Disturbance Waves in Compressible Boundary Layers," *Laminar-Turbulent Transition, IUTAM Symposium, Toulouse, France, 1989,* edited by D.Arnal and R.Michel, Springer-Verlag Berlin, 1990, pp 303-310.

[23] Fasel, H., Trumm, A. and Bestek, H."Direct Numerical Simulation of Transition in Supersonic Boundary Layer: Oblique Breakdown," *Transitional and Turbulent Compressible Flows, ASME FED-Vol. 151,* 1993, pp 77-92.

[24] Eibler, W. and Bestek, H., "Spatial Numerical Simulations for Nonlinear Transition Phenomena in Supersonic Boundary Layers," *Transitional and Turbulent Compressible Flows,* Vol. L. D. Kral and T. A. Zang, editors, pp. 69-76, FED-Vol. 151, ASME, 1993

[25] Eibler, W. and Bestek, H. "Spatial Numerical Simulations of Linear and Weakly Nonlinear Instabilities in Supersonic Boundary Layers," *Theoretical and Computational Fluid Dynamics,* Vol. 8, 1996, pp. 219 – 235.

[26] Adams, N. A. and Kleiser, L. "Numerical Simulation of Transition in a Compressible Flat Plate Boundary Layer,"*Transitional and Turbulent Compressible Flows, ASME FED-Vol. 151,* 1993, pp. 101-110.

[27] Adams, N. A., "Subharmonic Transition to Turbulence in a Flat-Plate Boundary Layer at Mach Number 4.5," *Journal of Fluid Mechanics,* Vol. 317, 1996, pp. 301-335.

[28] Pruett, C. D. and Chang, C.L. ,"A Comparison of PSE and DNS for High-Speed Boundary-Layer Flows," *Transitional and Turbulent Compressible Flows,* L. D. Kral and T. A. Zang, editors, pp. 57-67, FED-Vol. 151, ASME, 1993.

[29] Pruett, C. D., Zang, T. A., Chang, C. L. and Carpenter, M. H."Spatial Direct Numerical Simulation of High-Speed Boundary-Layer Flows, Part I: Algorithmic Considerations and Validation," *Theoretical and Computational Fluid Dynamics,* Vol. 7, 1995, pp. 49-76.

[30] Pruett, C. D. "Spatial Direct Numerical Simulation of Transitioning High-Speed Flows," *Transitional and Turbulent Compressible Flows,* L. D. Kral, E. F. Spina, and C. Arakawa, editors, pp. 63-70, FED-Vol. 224, ASME, 1995.

[31] Zhong, X. "High-Order Finite-Difference Schemes for Numerical Simulation of Hypersonic Boundary-Layer Transition," *Journal of Computational Physics,* Vol. 144, August 1998, pp. 662-709.

[32] Zhong, X. "Leading-Edge Receptivity to Free Stream Disturbance Waves for Hypersonic Flow Over A Parabola," *Journal of Fluid Mechanics*, Vol. 441, 2001, pp. 315-367.

[33] Augustinus, J., Hoffmann, K. A. and Harada, S.,"Numerical Solutions of Ideal MHD Equations for a Symmetric Blunt Body at Hypersonic Speeds," *AIAA Paper 98-0850,*1999.

[34] Gaitonde, D. V. "Development of a Solver for 3-D Non-Ideal Magnetogasdynamics,"*AIAA Paper 99-3610,* 1999.

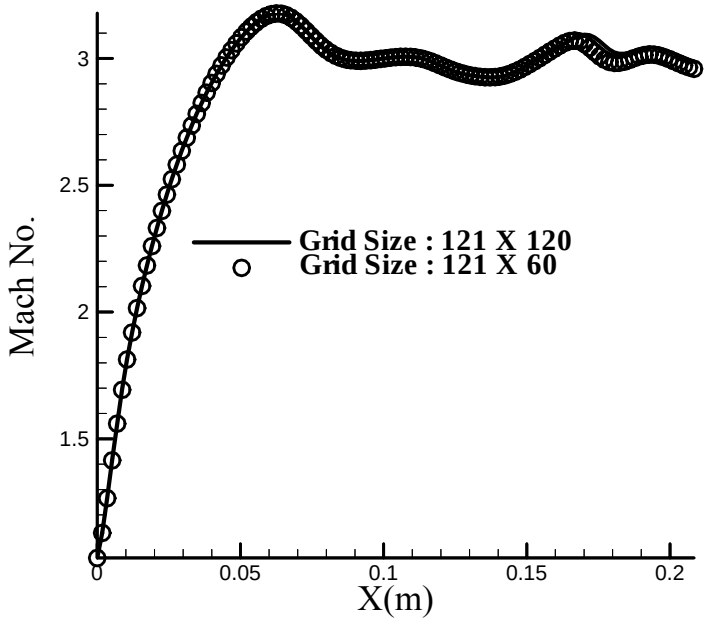


*(a)*

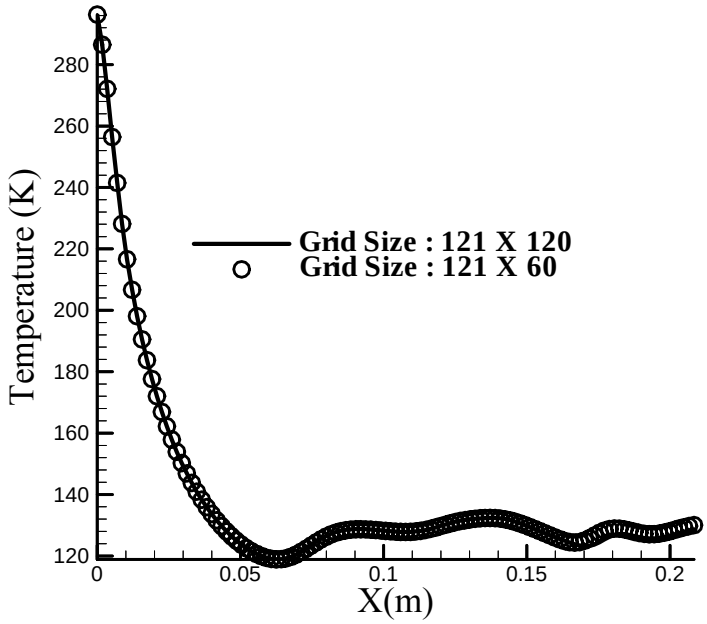


*(b)*

*Figure 1. The comparison of results from two different grid sizes, comparing the Mach number distribution at the centerline in figure 1(a) and temperature at the centerline in figure 1(b).*

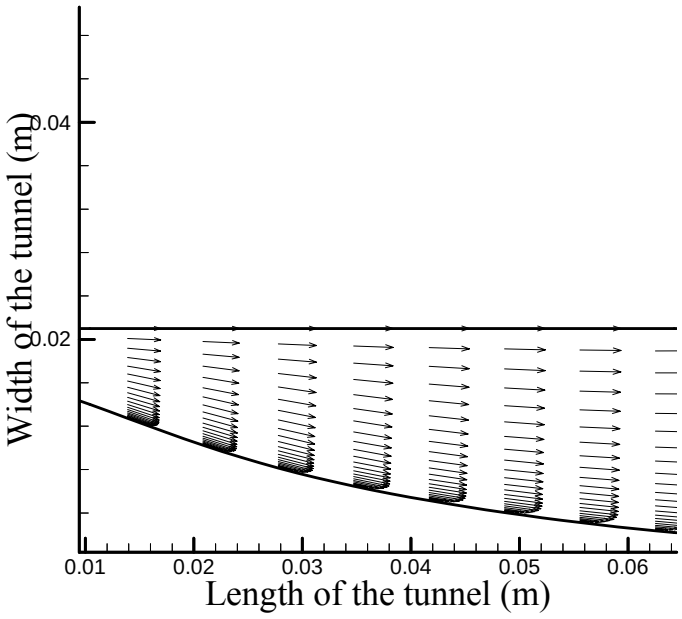


*(a)*

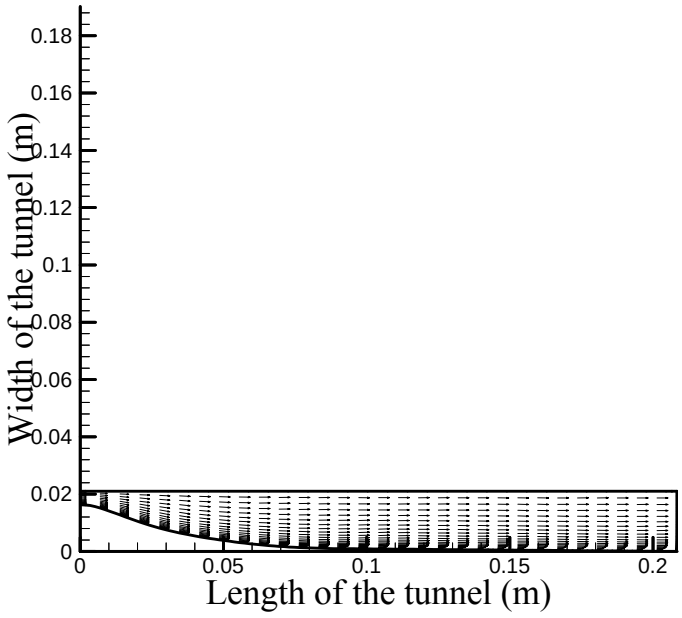


*(b)*

*Figure 2. The schematic of the velocity vectors in the tunnel without any imposed electromagnetic fields.*

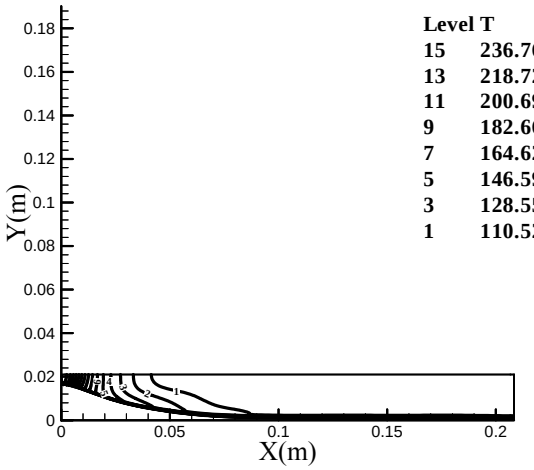


*(a)*

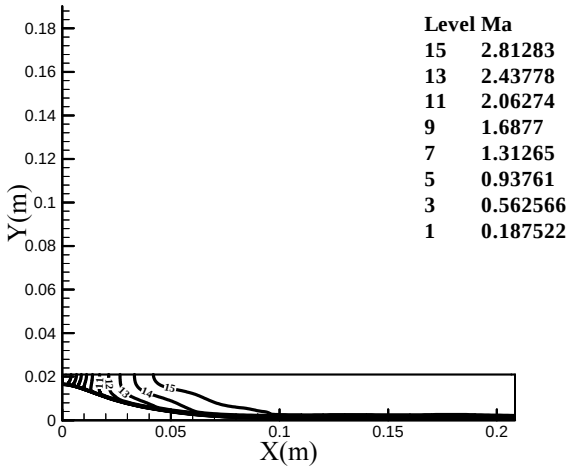


*(b)*

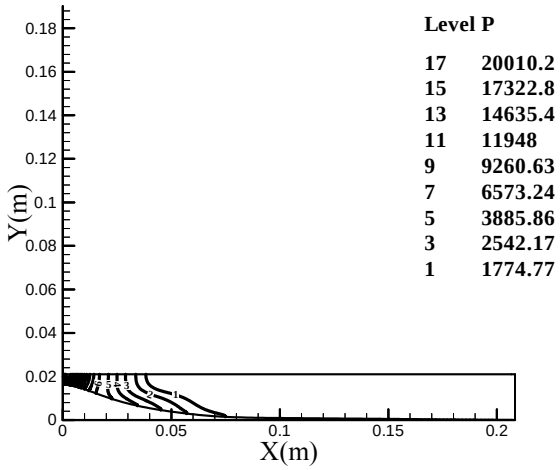


*(c)*

*Figure 3. Isocontours of Temperature, Mach number and Pressure throughout the tunnel in the absence of any external electromagnetic fields.*

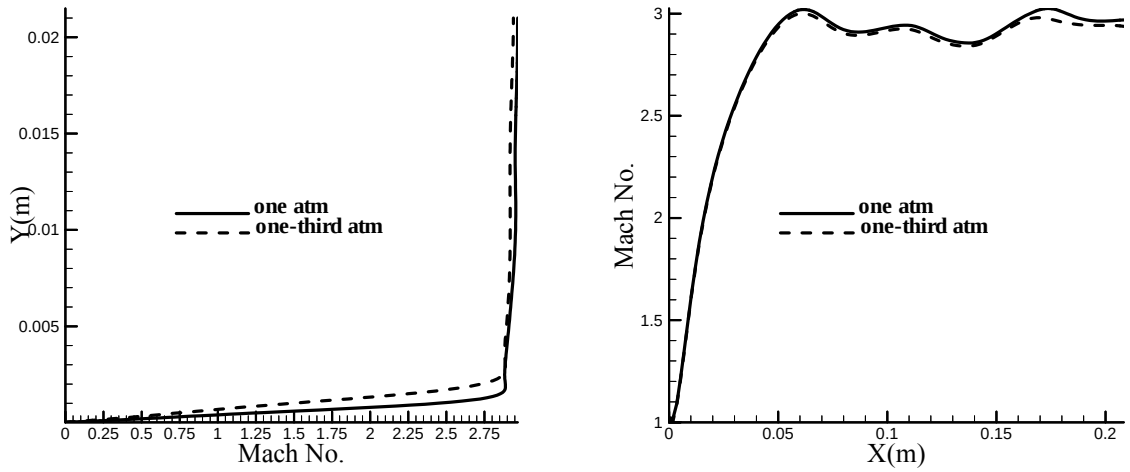


*(a)* *(b)*

*Figure 4. The effect of reducing the inlet stagnation pressure from one atmosphere to one-third atmosphere which leads to a significant increase in the boundary layer thickness without much difference on the Mach number profile at the centerline. The boundary layer profile shown here is at the exit of the tunnel.*

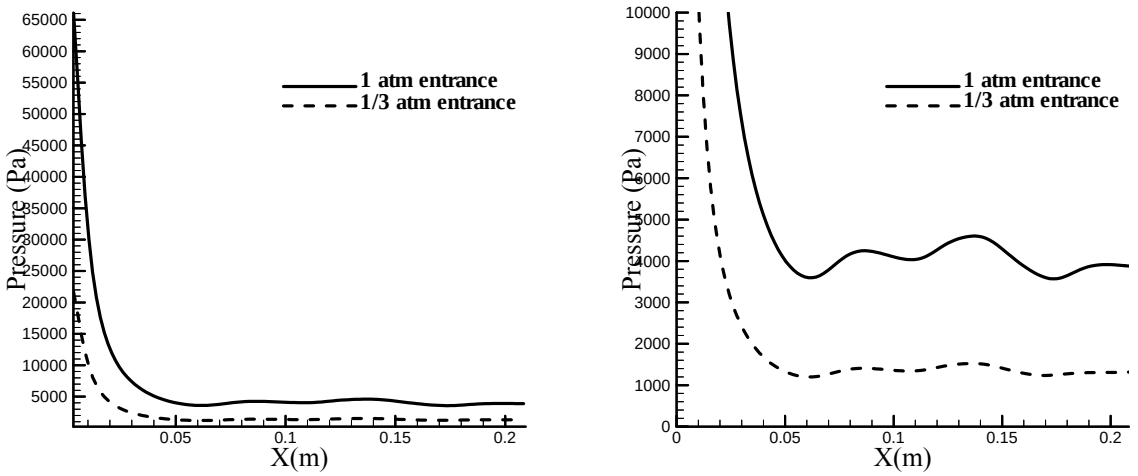


*(a)* *(b)*

*Figure 5. The effect of reducing the inlet stagnation pressure from one atmosphere to one-third atmosphere which leads to a significant alteration on the pressure distribution at the centerline.*

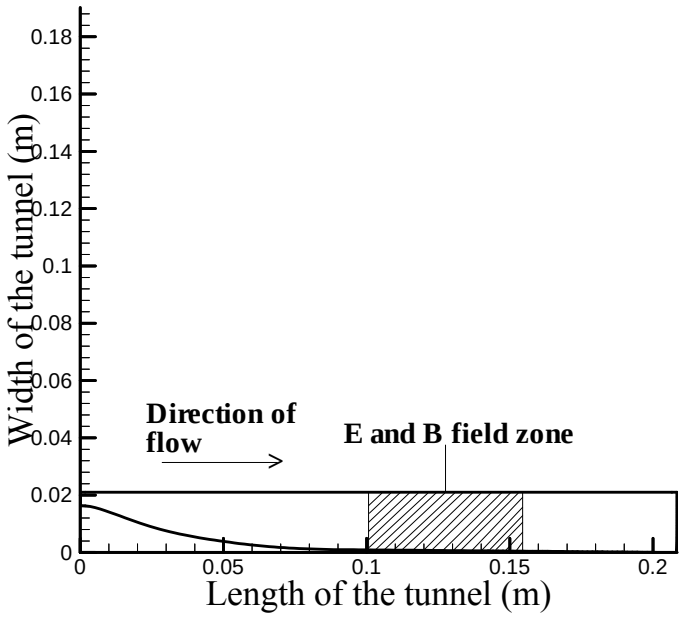


*(a)*

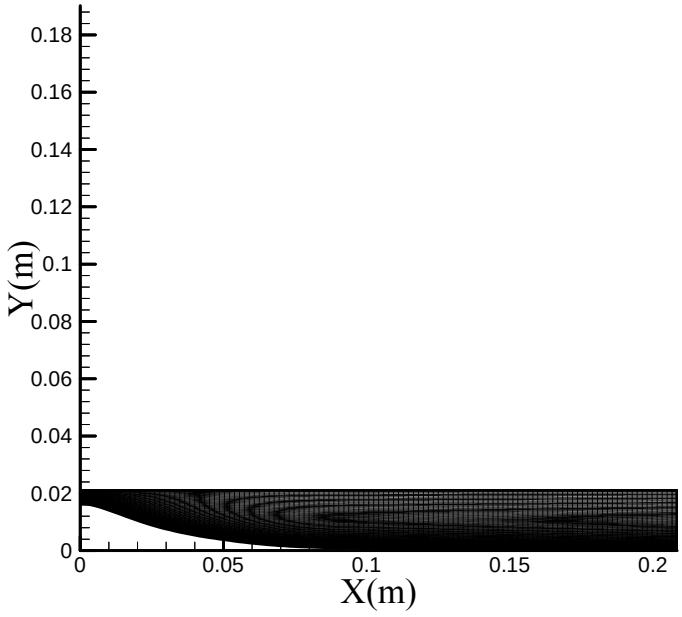


*(b)*

*Figure 6. These figures show the schematic of field locations in the setup and the two dimensional computational grid, respectively, used for calculating the flow fields.*

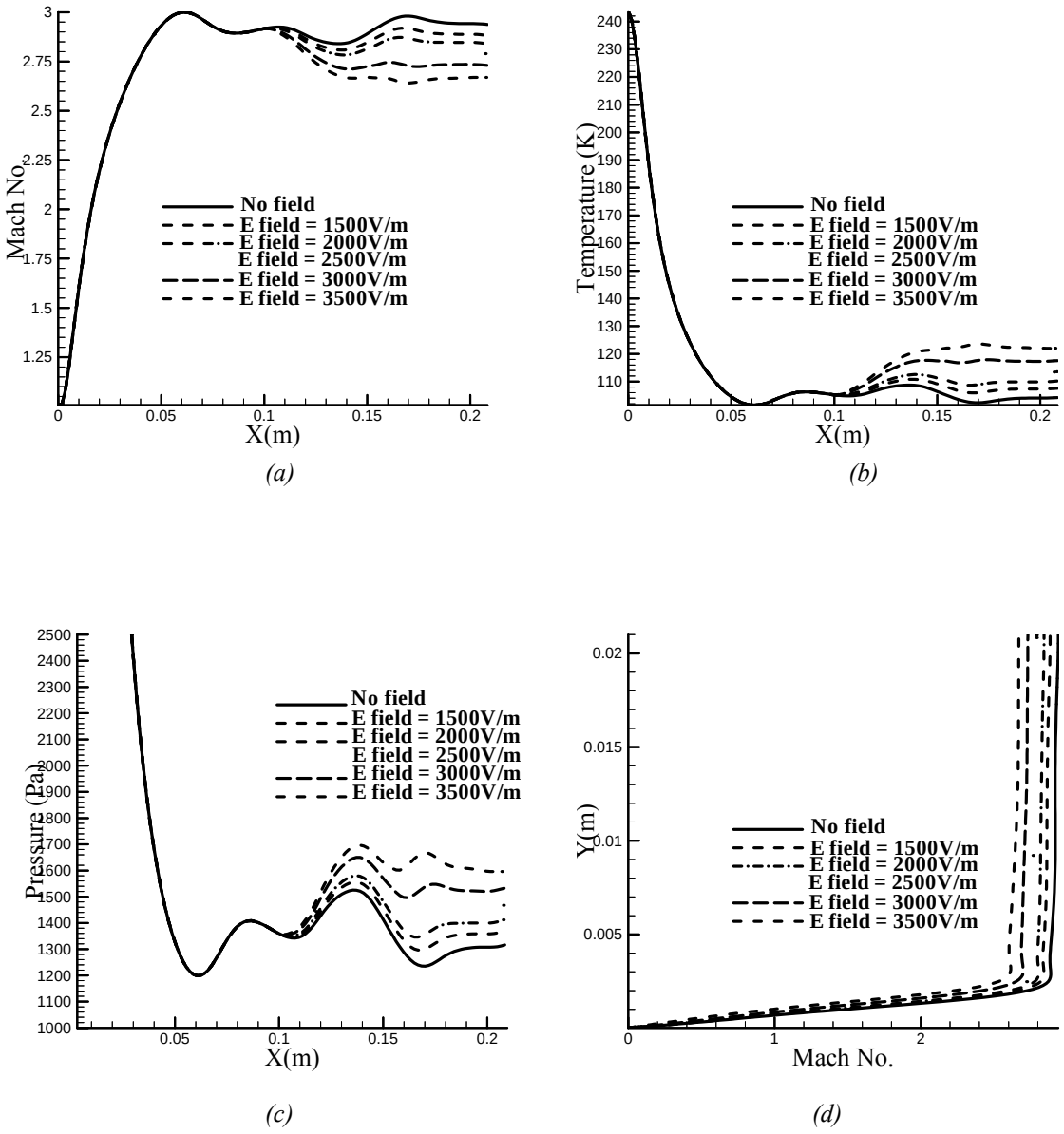


*Figure 7. The variations in the flow properties due to imposed electric fields, in the absence of magnetic fields.(a), (b)and (c) show the Mach number, temperature and pressure distribution at the centerline and (d) shows the boundary layer profiles at the exit of the tunnel.*

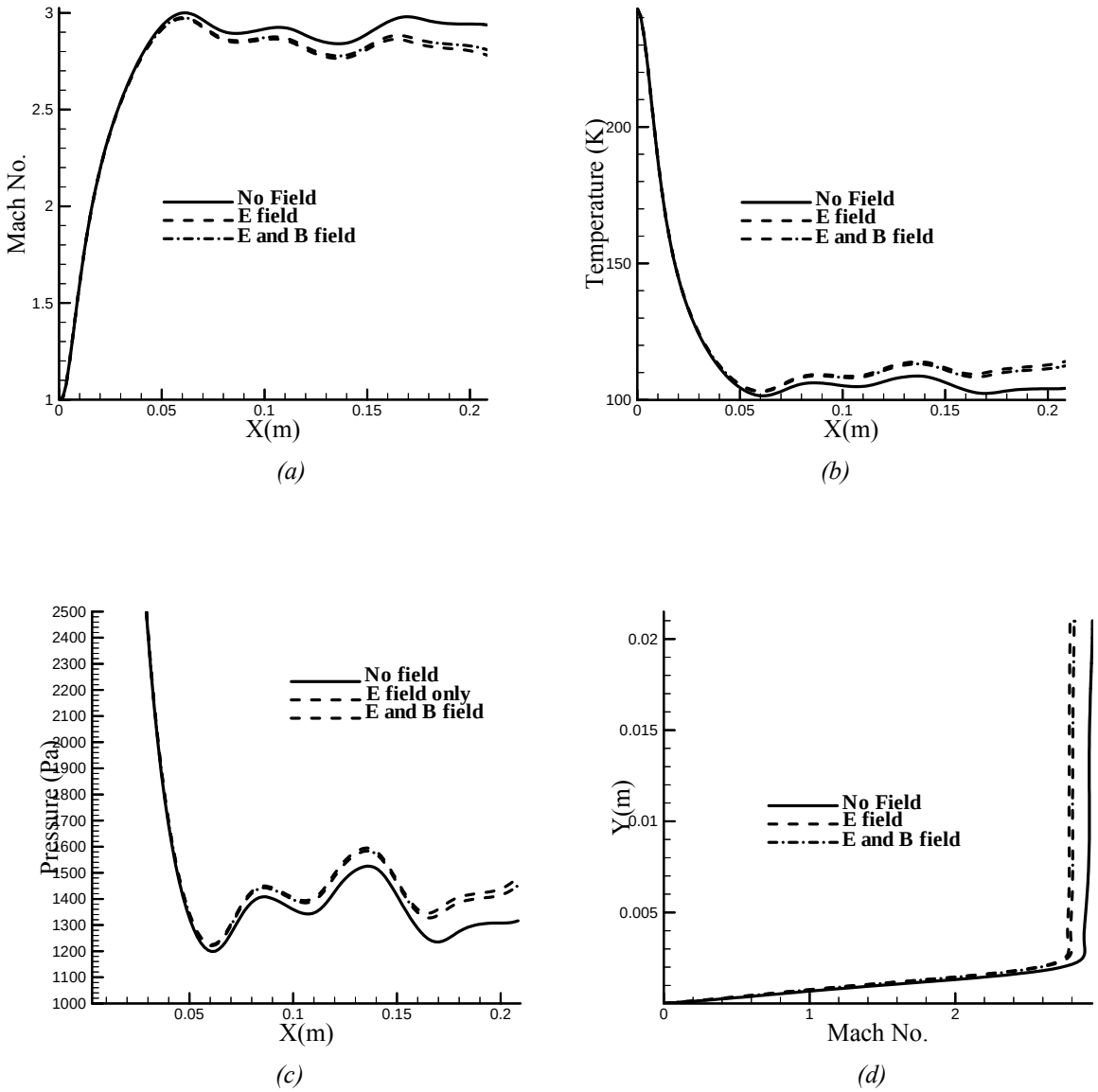


*Figure 8. The mitigating effect of the magnetic field on the joule heating shown here by comparing Mach number, temperature and pressure profiles at the centerline and Mach number profile at the tunnel exit respectively.*

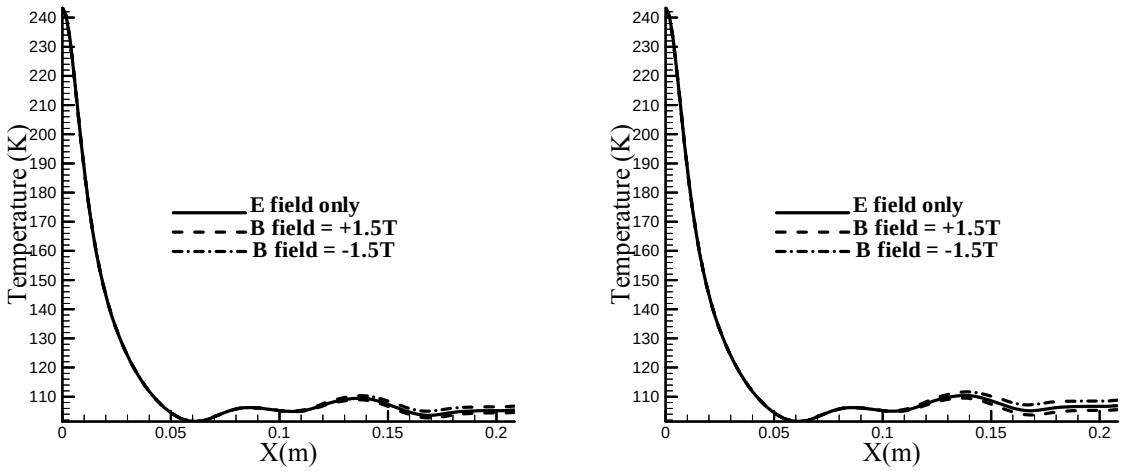


*Figure 9. The effect of reversing magnetic field direction on the temperature at the centerline with two different electric fields of 2000V/m and 3000V/m respectively. The magnetic field magnitude is fixed at 1.5T.*

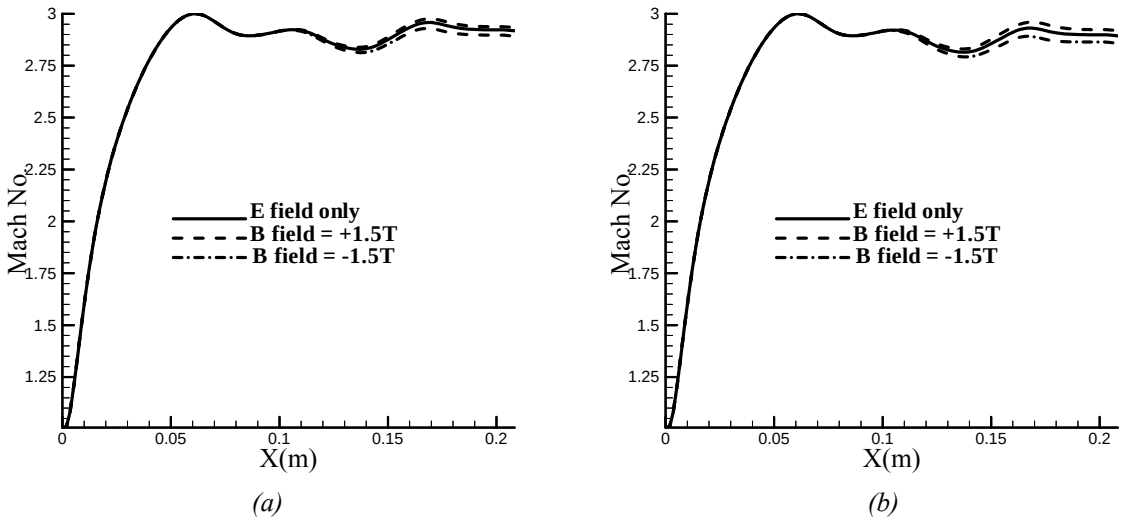


*Figure 10. The effect of reversing magnetic field direction on the Mach number at the centerline with two different electric fields of 2000V/m and 3000V/m respectively. The magnetic field magnitude is fixed at 1.5T.*

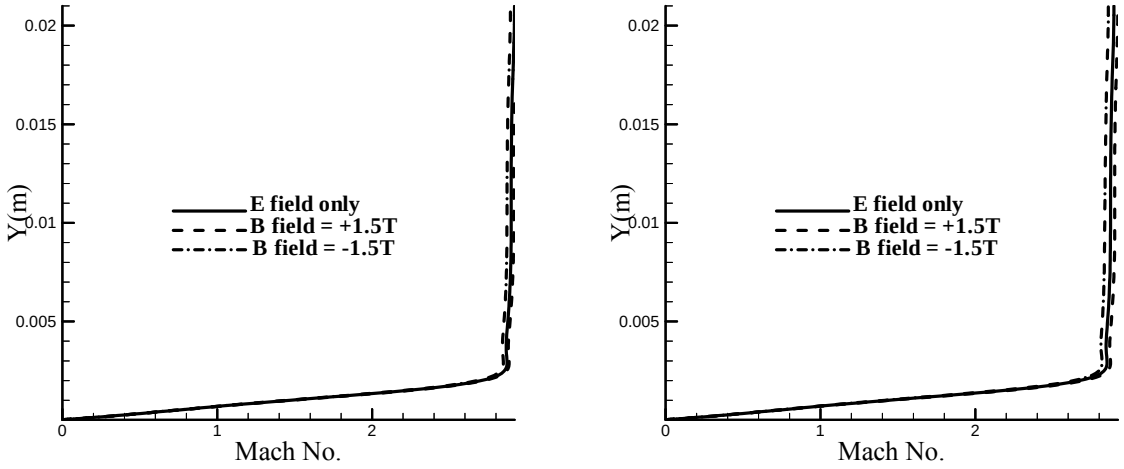


*Figure 11. The effect of reversing magnetic field direction on the Mach number at the tunnel exit with two different electric fields of 2000V/m and 3000V/m respectively. The magnetic field magnitude is fixed at 1.5T.*

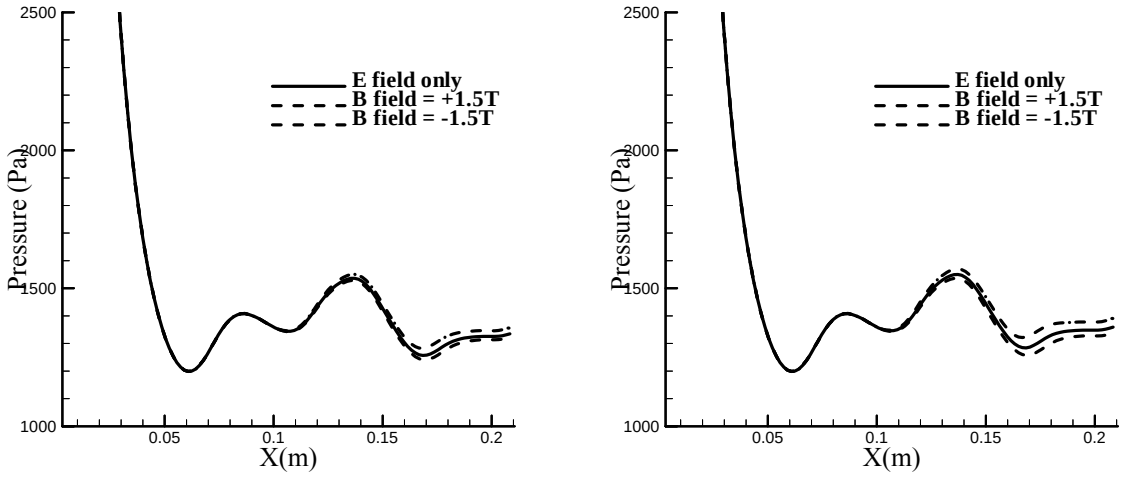


*Figure 12. The effect of reversing magnetic field direction on the Mach number at the tunnel exit with two different electric fields of 2000V/m and 3000V/m respectively. The magnetic field magnitude is fixed at 1.5T.*

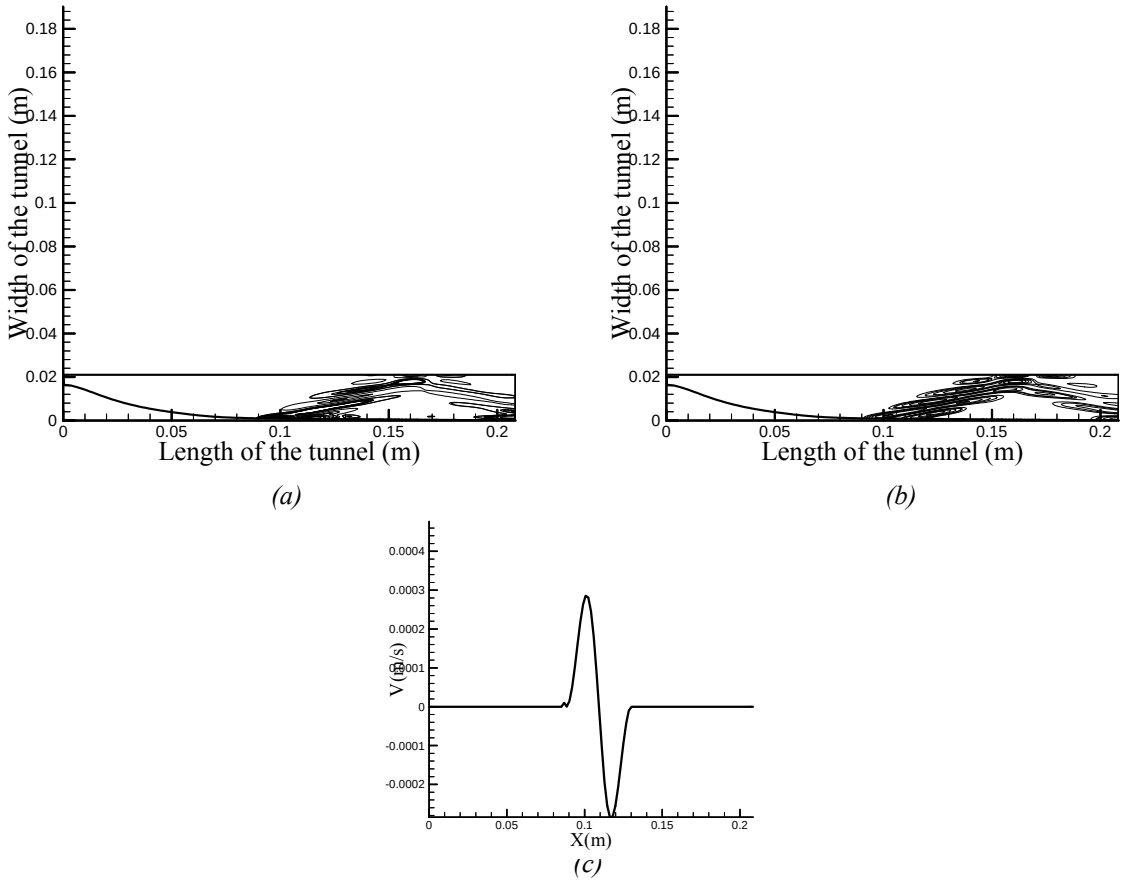


*Figure 13. The preliminary results of the Mach number and the pressure disturbance when a blowing and suction wall disturbance is imposed in the tunnel test section at 0.11m downstream of the tunnel entrance.*